Seismic Velocity Structure along the Western Segment of the North Anatolian Fault Zone Imaged by Seismic Tomography

Mohamed K. Salah[1]*, S. Sahin[2] and M. Kaplan[3]

[1] Earthquake Research Institute, University of Tokyo, Tokyo 113–0032, Japan
[2] Faculty of Engineering and Architecture, Suleyman Demirel University, Isparta, Turkey
[3] General Directorate of Disaster Affairs, Earthquake Research Department, Ankara, Turkey

Abstract

The three-dimensional P and S wave velocity structures of the crust of the central and western segments of the North Anatolian Fault Zone are determined by applying a tomography method to arrival times data generated by local earthquakes that occurred beneath the study area. From the obtained P and S wave velocity models, we further calculate Poisson's ratio for a more reliable interpretation of the imaged seismic anomalies. With the exception of high-velocity anomalies detected at a depth of 8 km, prominent low-velocity zones are clearly visible along most parts of the studied segment down to a depth of 25 km. High Poisson's ratio anomalies are widely distributed in most parts of the studied region. Seismic activity is more intense in the high-velocity and high Poisson's ratio zones, although it sometimes occurs in low-velocity areas. Large crustal earthquakes occur in areas characterized by a highly heterogeneous velocity structure, but with distinctly high Poisson's ratio anomalies. These results indicate that the active tectonics of this area are reflected in the seismic velocity structure, and that large crustal earthquakes occur generally in highly heterogeneous zones revealed by seismic tomography. These inferences are of great significance for understanding earthquake-generating processes in areas having intense seismic and tectonic activities such as the Anatolian plate.

Key words: Seismic tomography, Poisson's ratio, P wave velocity, S wave velocity, North Anatolian Fault Zone

1. Introduction

The North Anatolian Fault Zone (NAFZ) system (Fig. 1), about 1500-km long, delineates the northern boundary of the Anatolian Plate, and is characterized by a right-lateral strike slip motion (McKenzie, 1972; Barka and Gülen, 1988). In this complex tectonic environment, the collision of the Arabian, African, and Eurasian plates leads to a compressive regime to the east of the Anatolian block (creating mountain ranges such as the Zagros and the Caucasus), a right-lateral strike-slip fault zone to the north (which accommodates the westward escape of the Anatolian block (McKenzie, 1972; Sengör, 1979), and a subduction zone associated with back arc spreading in the Aegean Sea (McKenzie, 1972; Barka and Gülen, 1988) to the

southwestern boundary of the Anatolian block (Fig. 1). Due to the intense tectonic activity in this region (*e.g.,* Aktug and Kilicoglu, 2006), the NAFZ has been the locus of large seismic events in past centuries, which presents a major source of risk for the population (Provost *et al.,* 2003). These large earthquakes testify that the present-day high strain rate is accommodated seismically (Pucci *et al.,* 2006), and place this fault among the most active strike-slip faults worldwide (Ambraseys, 1970; Ambraseys and Finkel, 1995; Ambraseys, 2002).

Seismicity along the active segments of the NAFZ is characterized by frequent moderate to large earthquakes (M>7) with focal mechanisms that show essentially pure right-lateral strike-slip solutions
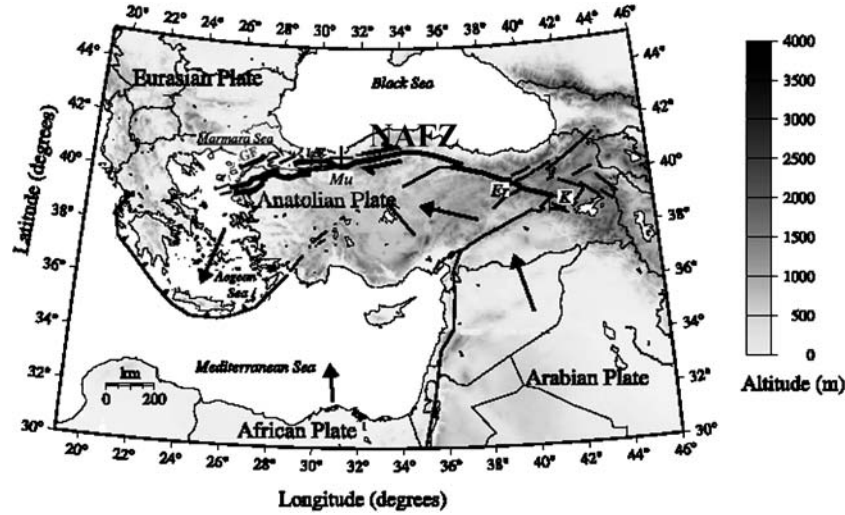
*e-mail: mksalah69@hotmail.com

Fig. 1. Simplified tectonic map of Turkey, Arabian, African, and Eurasian plates (Provost *et al.,* 2003). The black arrows show the directions of relative plate velocity, and the thick black line shows the location of the right-lateral strike-slip NAFZ. Epicenters of 17 August 1999 Gölcük earthquake and 12 November 1999 Düzce earthquake are shown by star and cross, respectively. Abbreviations are: (K) Karliova triple junction; (Er) Erzincan; (Mu) Mudurnu Valley; (IzF) Izmit fault; (GF) Ganos fault.

(*e.g.,* Canitez and Üçer, 1967; McKenzie, 1972; Zanchi and Anglier, 1993). The 1999 earthquakes are the most recent to occur on the NAFZ in the 20th century. The first of these earthquakes (Gölcük earthquake) occurred on 17 August, striking the Izmit region, west of the Marmara Sea. This Mw 7.4 (USGS) earthquake has a focal mechanism (Harvard CMT) that is consistent with a right-lateral movement along an E-W strike-slip fault. Maximum surface dextral offsets exceeded 5 m, and surface rupture extended along the fault for a total rupture length of ∼110 km (Barka, 1999; Barka *et al.,* 2000, 2002). Three months later, on 12 November (Muller *et al.,* 2003; Utkucu *et al.,* 2003), the Mw 7.1 Düzce earthquake occurred. The focal mechanism solution shows almost a pure, dextral strike-slip movement on an E-W nodal plane, dipping 54° to 64° to the north, with a rake between 177° and 167° (USGS, Harvard CMT (Tibi *et al.,* 2001)). This earthquake produced right-lateral surface ruptures over a total length of ∼40 km and a maximum dextral offset of 5 m (Akyüz *et al.,* 2000, 2002). As a result of these two large events, 20,000 people were killed and over 100,000 people were injured and/or lost their homes and property. The extent of the damage was mainly due to the dense population of the region. A very severe (Mw >7) earthquake is expected in the Marmara sea region within the next 30

years, which endangers the city of Istanbul, where over 10 million people live (*e.g.,* Rockwell *et al.,* 2001; Papazachos *et al.,* 2002; Gürer *et al.,* 2003). Improving our knowledge of the seismic velocity structure of the crust in which these large catastrophic events take place will contribute to a better understanding of the overall tectonics of this region and the forces triggering these earthquakes.

Although there have been extensive studies of the tectonics and near-surface geology of this unique region, research on deep crustal structure and earthquake activity has been hampered by the sparse coverage of seismic stations. Recently, Akyol *et al.* (2006) obtained a 1-D P-wave crustal velocity model for western Anatolia, which is characterized by crustal velocities that are significantly lower than average continental values. It shows four layers down to a depth of 29 km (the assumed Moho depth), with a velocity of 6.25 km/s at depths between 15 and 21 km and a velocity of 6.43 km/s for the lowermost crust (depth range 21–29 km). The velocity at the shallowest layer (depth < 3 km), however, is poorly constrained due to the lack of head waves and refracted waves at the surface in the data set they used. The low velocities might be associated with high crustal temperatures, a high degree of fracture, or the presence of fluids at a high pore pressure in the crust (Akyol *et*

al., 2006). In this study we investigate three-dimensional velocity and Poisson's ratio structures of the crust of this area, and try to correlate them with other geophysical observations that will strengthen our current knowledge of the region, thus helping to mitigate geoseismic hazards.

2. Data

In this study we used 3733 events that occurred near or to the north of the western segment of NAFZ (Fig. 2a). We used 1051 aftershocks of the August 17, 1999 Golcuk earthquake ($M_w = 7.4$) between August 17

and September 15, 1999 and 1079 aftershocks of the November 12, 1999 Duzce earthquake ($M_w = 7.1$). These events were recorded by 14 Sakarya-Bolu Microearthquake Recording Network (Sabonet) seismic stations and 1 Turkish National telemetric earthquakes network (Turknet) permanent station belonging to the Turkish General Directorate of Disaster Affairs (Fig. 3). The remaining 1603 events are from background seismicity in the area, and occurred between 1998 and 2003; and were also recorded by the above-mentioned seismic networks. These events are located between latitudes $39.5°–41.5°$N and longitudes $28°–32°$E with focal depths down to about 35 km (Fig. 2a). The uneven distributions of both the seismic stations and the seismic events in the study area impose limitations on the resolution scale of the anomalies obtained, as is explained in the following sections. The error in the hypocentral locations does not exceed 2.5 km for all events. Earthquakes tend to cluster around the two 1999 main shocks, but we also selected additional events around these clusters to get a more uniform distribution of hypocenters in the study area. The selected 3733 events generated 20702 P and 14148 S arrivals recorded by the 15 seismic stations shown in Fig. 3. The accuracy of arrival times is estimated to be less than 0.15 s for P wave data and somewhat larger (< 0.25 s) for the S wave data. We examined all the residuals stepwise with respect to the assumed initial velocity model, and removed data with residuals beyond the limit ± 1 s.
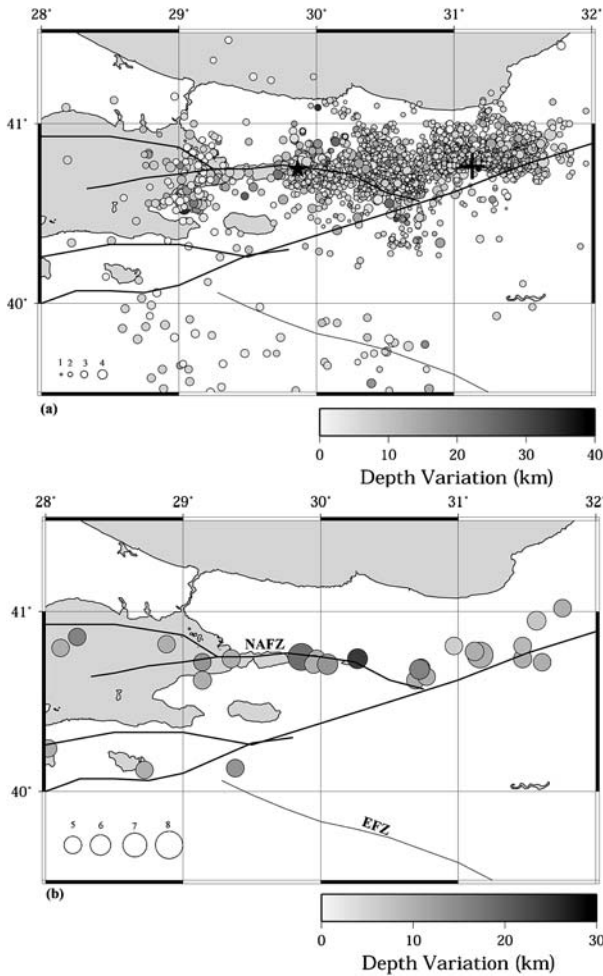
To study the relation between the nucleation

Fig. 2. (a) The epicenteral distribution of the 3733 events used in this study that occurred along the northwestern side of the NAFZ. Star is the epicenter of 17 August 1999 Gölcük earthquake and cross is the epicenter of 12 November 1999 Düzce earthquake. (b) The distribution of large earthquakes that occurred along the NAFZ ($M \geq 5.0$) since 1980. Thick and thin lines denote the North Anatolian Fault Zone (NAFZ) and the Eskisehir Fault Zone (EFZ), respectively.
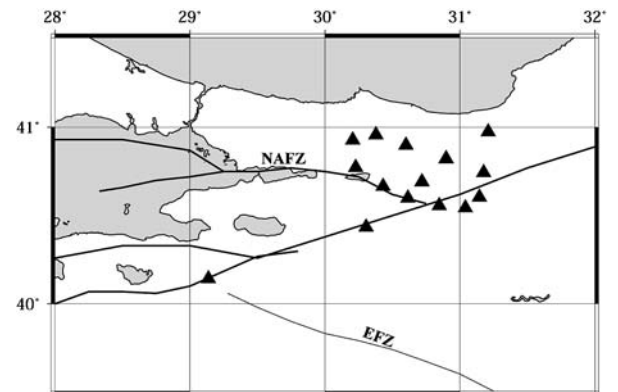

Fig. 3. Locations of seismic stations used in the present study that belong to Sabonet and Turknet seismic networks. Thick and thin lines denote the North Anatolian Fault Zone (NAFZ) and the Eskisehir Fault Zone (EFZ), respectively.

zones of large crustal earthquakes (M≥5) and the seismic velocity and Poisson's ratio anomalies obtained, we also collected data on 26 events that occurred in the study area starting from January 1980 up to December 2005, from the earthquake catalog of the National Earthquake Information Center (NEIC), U.S. Geological Survey (Fig. 2b). A close inspection of the distribution of the epicenters of these large events suggests that they occur mainly due to movements along the NAFZ as explained in the previous section.

3. Method

The seismic tomography method was first developed by Aki and Lee (1976). Subsequently, many researchers have successfully improved this technique and applied it to various regions around the world (*e.g.*, Hirahara, 1977; Thurber, 1983; Spakman and Nolet, 1988; Zhou and Clayton, 1990, Zhao *et al.*, 1992, 1994; Nakajima *et al.*, 2001; Mishra *et al.*, 2003). In this study, we use the tomographic method of Zhao *et al.* (1992), which has been applied to many regions having different tectonic circumstances (*e.g.*, Zhao and Kanamori, 1995; Zhao *et al.*, 1996, 1997, 2001; Serrano *et al.*, 1998, 2002a, b; Kayal *et al.*, 2002). The method uses an efficient 3-D ray tracing scheme to compute travel times and ray paths. We adopted a grid spacing of 0.2° in the horizontal direction and 6–15 km in the depth direction (Fig. 4). Velocities at grid nodes are taken as unknown parameters, and the velocity at any point in the model is calculated by linearly interpolating the velocities at the eight grid nodes surrounding that point. For more details about the method, see Zhao *et al.* (1992, 1994).

The interpretation of tomographic images is usually nonunique, because any given velocity anomaly can be attributed to either a thermal or a chemical variation. For this reason, it is generally useful to consider some other physical parameters for a more reliable interpretation of the anomalies obtained in terms of tectonic and geodynamic implications. Compared to the seismic velocity itself, the Poisson's ratio (or Vp/Vs ratio) is a better indicator of the content of fluids and/or magma (Zhao and Negishi, 1998; Kayal *et al.*, 2002; Takei, 2002; Salah and Zhao, 2003; Nakajima *et al.*, 2001, 2005) or serpentinization (Kamiya and Kobayashi, 2000; Christensen, 1996). Therefore, after Vp and Vs models are calculated from travel
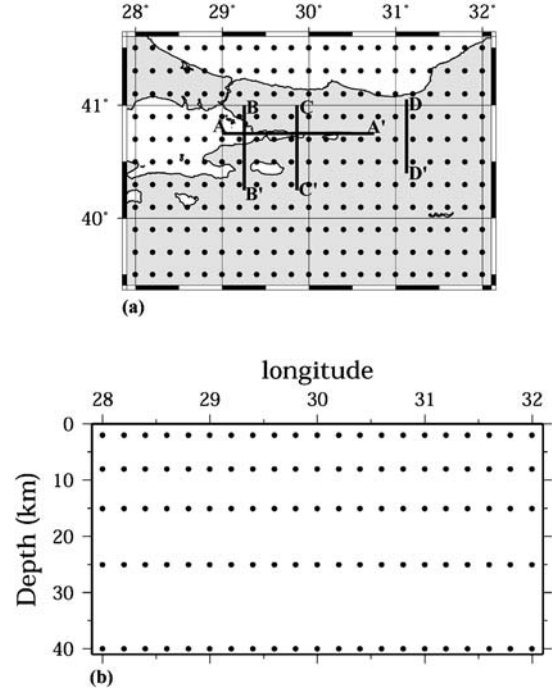

Fig. 4. 3-D configuration of the grid net adopted for the present study in horizontal (a), and depth (b) directions. Grid spacing is 0.2° in the horizontal direction and 6–15 km in the depth direction. Straight lines in (a) show the location of vertical cross-sections in Figs. 13–16.

time inversions, we use the following relation:

$$(Vp/Vs)^2 = 2(1-\sigma)/(1-2\sigma),$$

to compute the Poisson's ratio (σ).

The selection of the initially used velocity model is an important step in any tomographic inversion because it generally affects the amplitude and distribution of the velocity anomalies obtained. We adopted a crustal velocity model that is slightly different from the model determined by Akyol *et al.* (2006) for western Anatolia as our initial P wave velocity model. Their model shows four layers down to a depth of 29 km (the assumed Moho depth), with a velocity of 6.25 km/s at depths between 15 and 21 km and a velocity of 6.43 km/s for the lowermost crust (depth range 21–29 km). The velocity at the shallowest layer (depth <3 km), however, is poorly constrained due to the lack of head waves and refracted waves at the surface in the data set they used. The model we used in our study, on the other hand, is even simpler. We assumed velocities of 5, 5.9, 6.0, 6.55, and 7.75 km/s at depths of 5, 10, 15, 25, and 40 km,
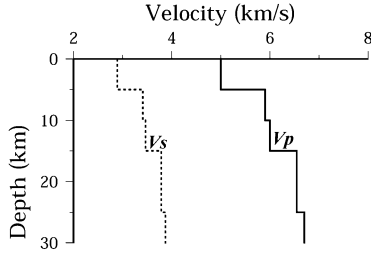
Fig. 5. Initial P wave (solid line) and S wave (dashed line) velocity models adopted for the present study.

respectively (Fig. 5). Because there are almost no studies of S wave velocity structure in this area, we used the relation: Vs＝Vp/1.73, to derive the initial S wave velocity model. We checked a number of slightly different initial velocity models, but finally selected the above-mentioned one because we found that it gives the minimum RMS travel time residual.

4. Resolution and Results

Before describing the main features of the results, we show the results of a checkerboard resolution test (CRT), (Inoue et al., 1990; Zhao et al., 1992, 1994) to demonstrate the reliability of the tomographic images obtained. The values of assumed checkerboard-type perturbations assigned to grid nodes are ±3%; the image of which is straightforward and easy to remember. Synthetic arrival times are then calculated for the checkerboard model. Numbers of stations and events with their exact locations in the synthetic data are taken to be the same as those in the real data set.

The CRT results for the P and S wave velocity structures at four crustal depth slices are shown in Figs. 6 and 7, respectively. The resolution is particularly good where many ray paths (event-station pairs) are traversing. At a depth of 2 km, there is good resolution in the areas where the seismic stations are located, and most of the input synthetic anomalies are well recovered. The surrounding parts have relatively poor resolution, especially where no events are located. This is due to insufficient ray paths criss-crossing there. For deeper layers (depths 8, and 15 km), the resolution is reliable only near the station locations and the seismically active regions (Figs. 6 and 7). Some parts of the study area have a reasonable resolution at a depth of 25 km because of sufficient lengths and directions of both horizontal

and vertical rays passing at this depth.

The final inversion results were obtained after two iterations. The P and S wave root-mean-square (RMS) travel time residuals calculated after these iterations were 0.27 and 0.30 s, respectively. In the following paragraphs we discuss the results of Vp, Vs, and Poisson's ratio only in areas having a reliable resolution.

Figures 8 and 9 show velocity perturbations relative to the initial velocity models of the P and S waves at depths of 2, 8, 15, and 25 km, respectively, together with the distribution of seismicity around the studied depth slice. The locations of the epicenters of the two large 1999 earthquakes are also shown. Fig. 10, on the other hand, shows perturbations of Poisson's ratio at the same depths. To study the relation between the nucleation zones of large earthquakes (M≥5) and the imaged anomalies, we also plot their epicentral distribution superimposed on the velocity and Poisson's ratio structures at 8 and 15 km depths (Figs. 11, and 12) because the focal depths of most of these events are around 10 km. In the following paragraphs, we describe the main features of our results.

At the shallowest layer (2 km depth), the velocity structure is generally heterogeneous, having strong lateral variations amounting to ±6%. A low P and S wave velocity anomaly is detected at the central portion of the study area (between longitudes 30 and 31.5°E) with some portions having a high P wave velocity. This low-velocity zone has a high Poisson's ratio, and is characterized by intense seismic activity (Figs. 8, 9, and 10). This heterogeneous structure continues down to a depth of 8 km, but is dominated by higher than average velocities. The amplitude of the high S wave velocity anomaly is much lower than that of the P wave, and sometimes the S wave velocity is lower than the average at the margins of the well-resolved zone. This is also reflected in the high Poisson's ratio anomalies seen in most parts. Seismic activity is relatively intense around this depth slice, and occurs mostly in the zone of average to high velocities and average to high Poisson's ratio with minor exceptions.

At depths of 15 and 25 km, prominent low P and S wave velocities are widely seen in most parts of the study area (well-resolved zone). Poisson's ratio is higher than average at a depth of 15 km, but is gener-
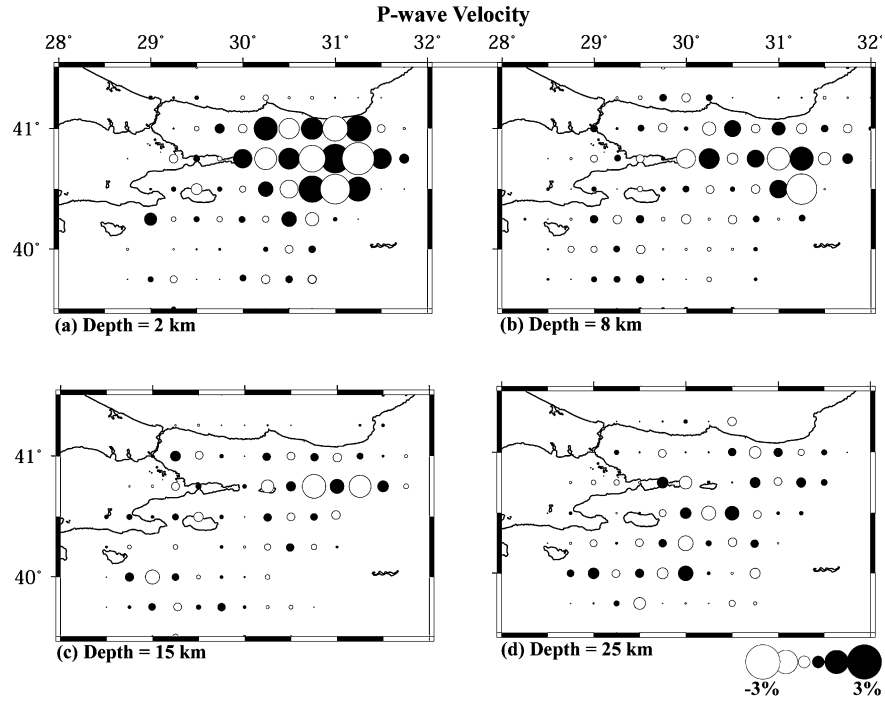
P-wave Velocity

Fig. 6. Results of a checkerboard resolution test for P wave velocity structures at four crustal depths. The grid spacing is 20 km. Filled and open circles show high and low velocities, respectively. Perturbation scale is shown at the lower right.
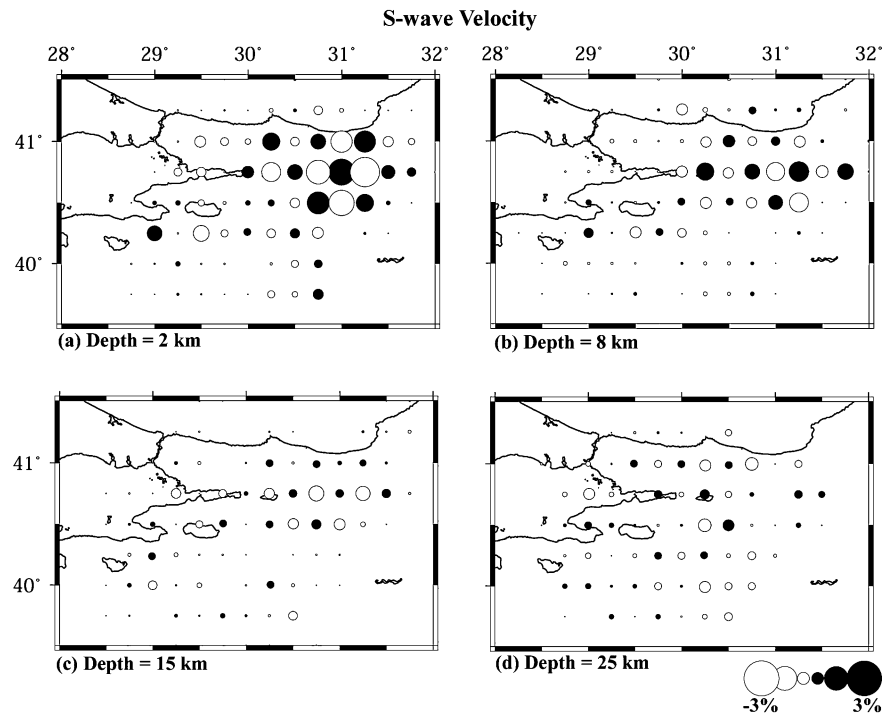
S-wave Velocity

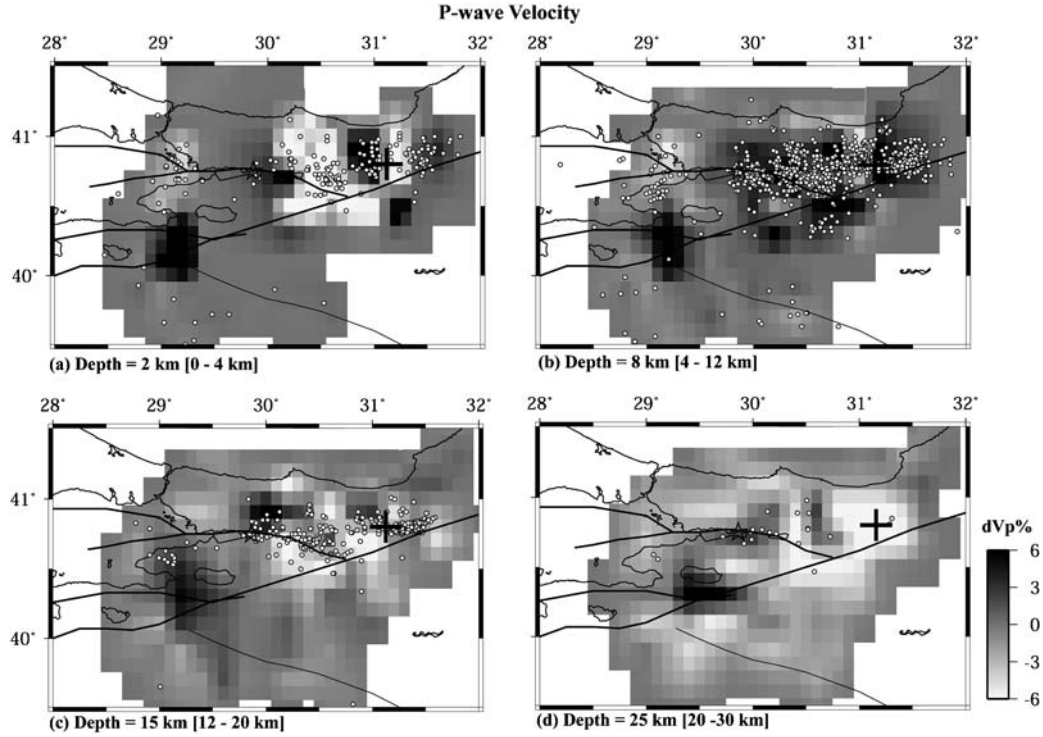Fig. 7. The same as Fig. 6, but for S wave velocity.

P-wave Velocity

Fig. 8. P wave velocity perturbations at depths of 2, 8, 15, and 25 km, respectively. White circles denote seismicity in the depth range shown between brackets below each map. Dark and light gray colors denote high and low velocities, respectively. The perturbation scale is shown to the right. Thick and thin lines denote the North Anatolian Fault Zone (NAFZ) and the Eskisehir Fault Zone (EFZ), respectively. Star and cross denote the epicenters of the 17 August 1999 Gölcük and the 12 November 1999 Düzce earthquakes, respectively.
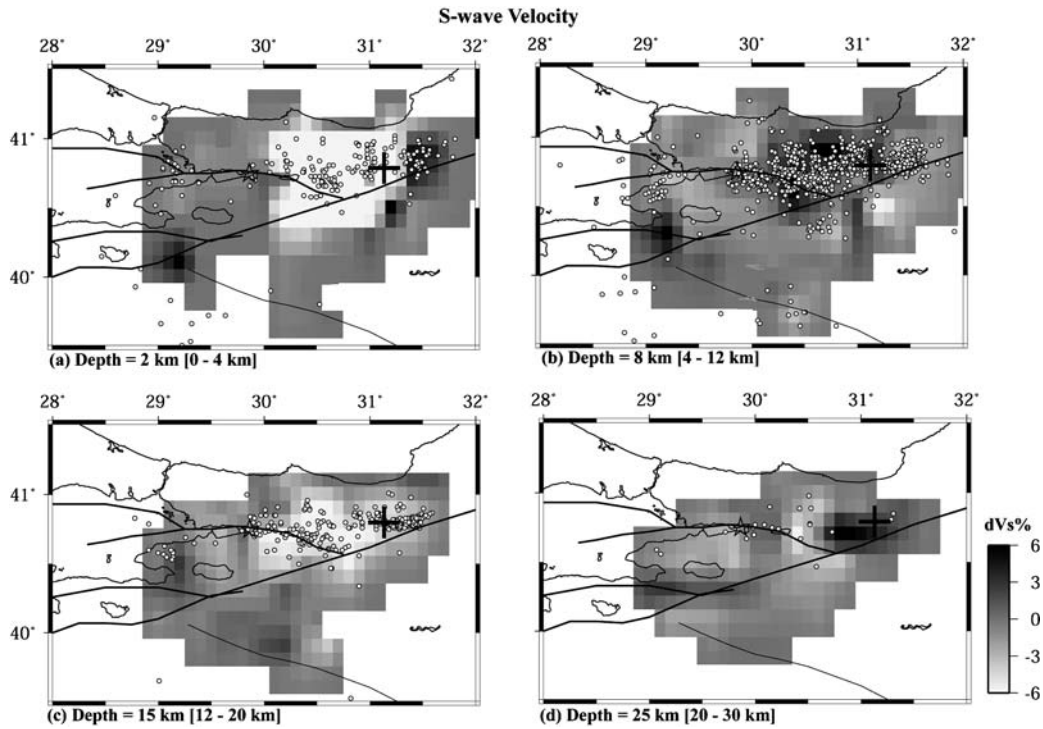
S-wave Velocity

Fig. 9. The same as Fig. 8, but for S wave velocity.
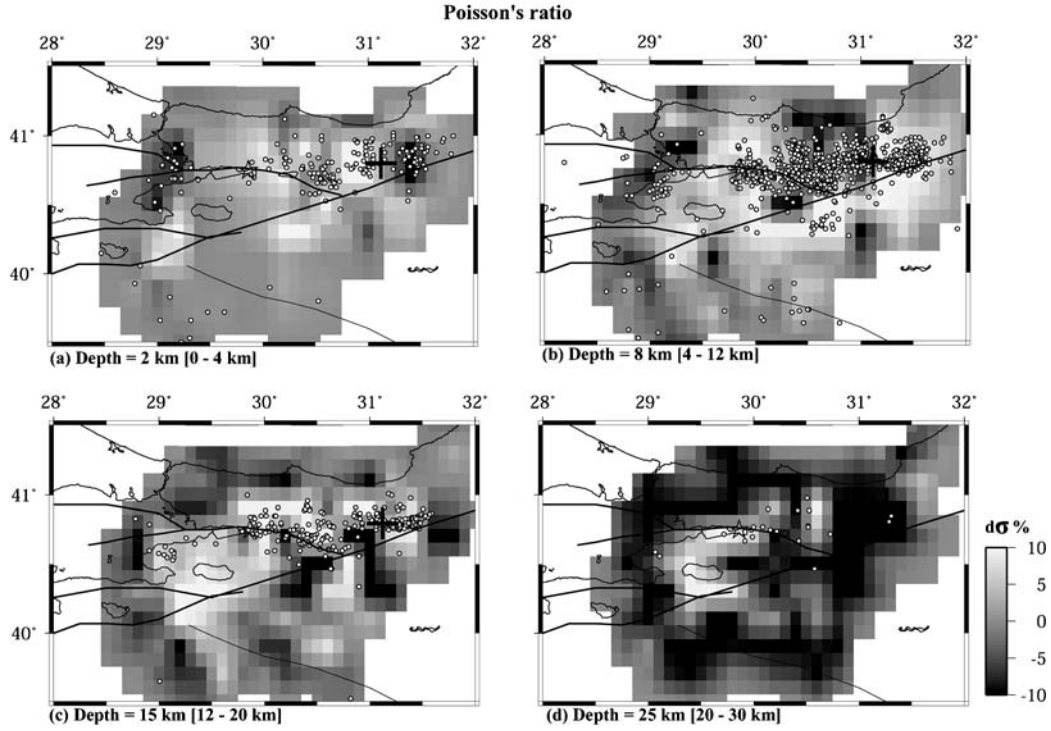
Poisson's ratio

Fig. 10. Distribution of Poisson's ratio perturbations at four depth slices. Light and dark gray colors denote high and low Poisson's ratios, respectively. Other details are similar to those of Fig. 8.

ally low at a depth of 25 km with the exception of the zone near the epicentral area of the 17 August, 1999 Golcuk earthquake. Seismic activity is also concentrated along the zones of low to average velocity/average to high Poisson's ratio.

In Figs. 11 and 12, we plot the seismic velocity and Poisson's ratio structures at depths of 8 and 15 km along with the epicentral distribution of the large crustal earthquakes. It is clear that the majority of the large events occur in the highly heterogeneous zones dominated by high velocities at a depth of 8 km, which is underlained by lower velocity zones at a depth of 15 km. The amplitude of the low S wave velocity zone, however, is higher, which is reflected in the prominent higher than average Poisson's ratios at the two depth slices. These results imply that fluids might be involved in triggering large events in this tectonically active region, as is explained later.

The velocity and Poisson's ratio structures described before are also illustrated along vertical cross-sections AA', BB', CC', and DD' (Figs. 13–16), which run either in the E-W or N-S directions (see Fig. 4 for the location of cross-sections). Cross-sections AA' and CC' pass through the hypocenter of the 17 August,

1999 Golcuk earthquake, while cross-section DD' passes through the hypocenter of the 12 November, 1999 Duzce earthquake. The velocity and Poisson's ratio structures are very heterogeneous at the top 10 km depths, but at deeper levels, low-velocity/high Poisson's ratio anomalies dominate. The hypocenters of the two large 1999 events are located in distinctive zones characterized by average P wave velocity, low S wave velocity, and high Poisson's ratio. The background seismic activity and the majority of the large earthquakes occur also in zones dominated by average P wave velocity, low S wave velocity, and high Poisson's ratio. We discuss the implications of these observations in the following paragraphs.

5. Discussion

5.1 Large earthquakes along the NAFZ

The NAFZ is an active right-lateral system, which is bound to the north by the westward extruding Anatolian block (McKenzie, 1972; Sengör, 1979; Barka, 1992; Saroglu et al., 1992). Since the Middle/Late Miocene (13–5 Ma) the NAFZ has accumulated a geologic displacement on the order of 85–120 km (Seymen, 1975; Sengör, 1979; Barka, 1981; Barka and
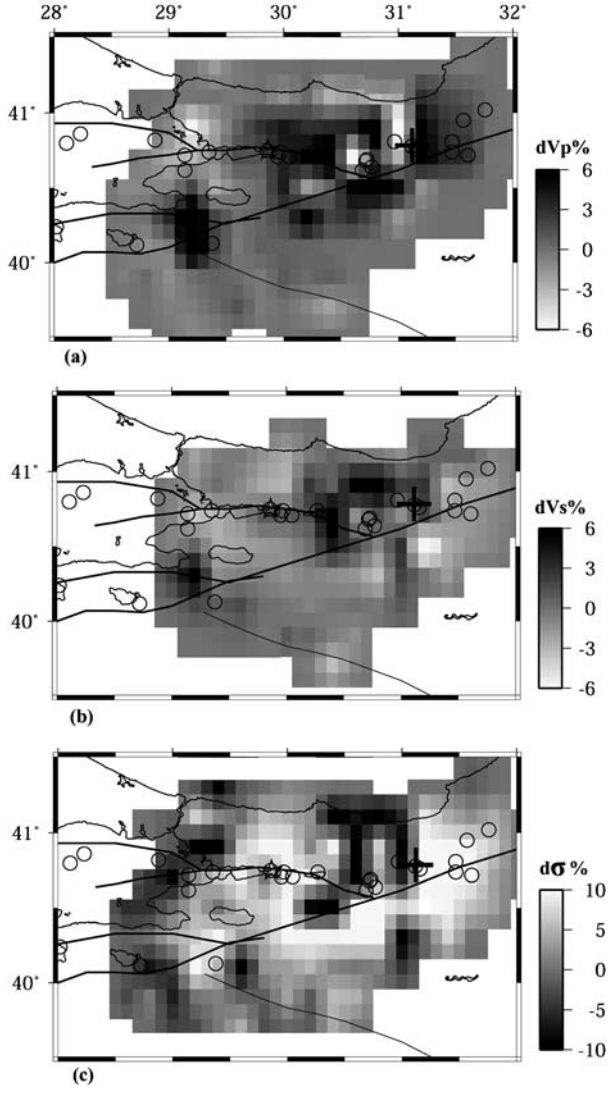
Fig. 11. P wave velocity (a), S wave velocity (b), and Poisson's ratio (c) perturbations at a depth of 8 km together with the epicenteral distribution of large earthquakes (see text for details). Other details are similar to those of Fig. 8.

Fig. 12. The same as Fig. 11, but at a depth of 15 km.

Hancock, 1984; Westaway, 1994; Armijo *et al.,* 1999; Hubert-Ferrari *et al.,* 2002). This displacement translates into a long-term and short-term geologic slip rate of 0.5–0.8 cm/yr (Tokay, 1973; Seymen, 1975; Barka and Hancock, 1984) and 1.8 cm/yr (Hubert-Ferrari *et al.,* 2002), respectively. Conversely, GPS networks have measured present-day strain rates in the northern part of the Anatolian block that reach ∼2–3 cm/yr (Reilinger *et al.,* 1997, 2000; Straub *et al.,* 1997; McClusky *et al.,* 2000; Kahle *et al.,* 1999, 2000). To the east of the town of Bolu, the NAFZ is formed by a main single trace, but to the west it splays into
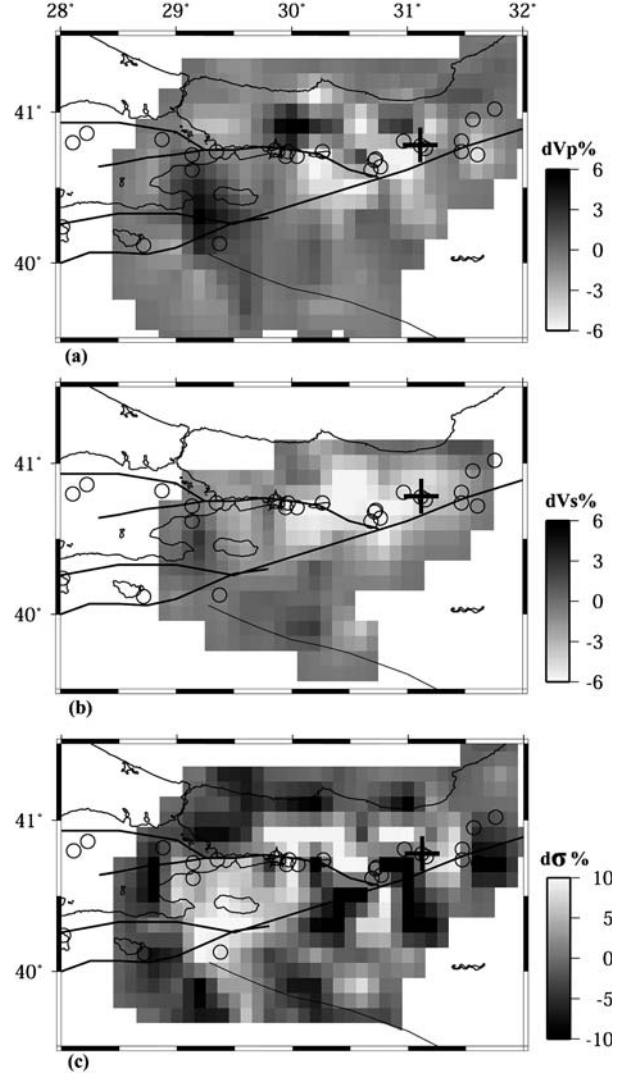
two main strands, the Duzce and the Mudurnu fault segments, where GPS data indicate that the former accommodates up to 10 mm/yr (Ayhan *et al.,* 1999). Farther west, the NAFZ splays again into three major strands and the northernmost one is considered to accommodate most of the present-day strain (Barka and Kadinski-Cade, 1988; Straub *et al.,* 1997).

The preceding paragraphs show a high rate of seismic activity along the NAFZ, which is also clear from the distribution of the seismic events used in this study (Fig. 2), most of which are aftershocks of the two large 1999 earthquakes (see section 2). The highly heterogeneous seismic velocity and Poisson's ratio crustal structures obtained in this study are consistent with this unstable seismo-tectonic setting. The majority of large crustal earthquakes oc-
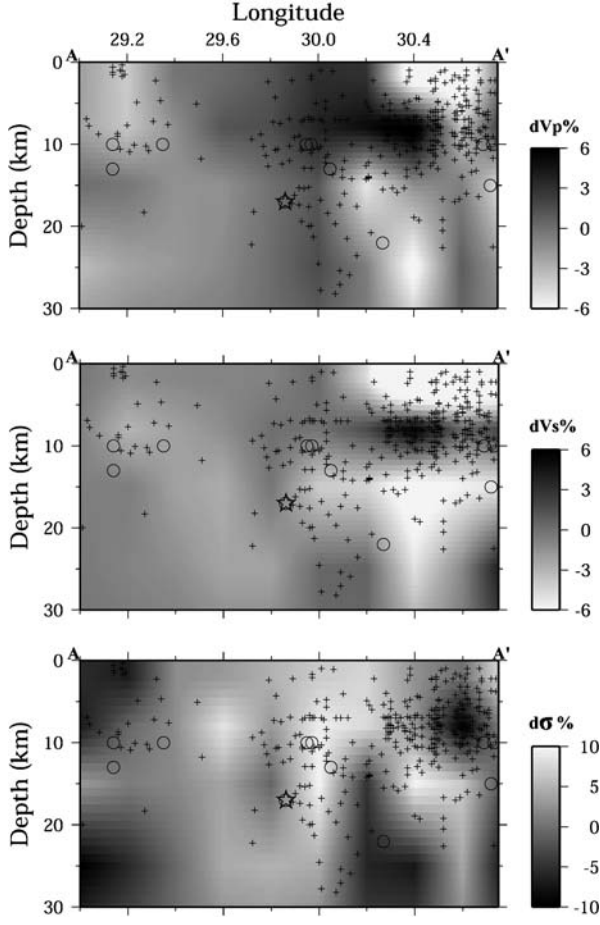
Fig. 13. Vertical cross-sections of P wave velocity, S wave velocity, and Poisson's ratio structures along line AA' (see Fig. 4 for the location of the cross-sections). Low velocities and high Poisson's ratios are shown by light gray, whereas high velocities and low Poisson's ratios are shown by dark gray. Star denotes the hypocenter of the 17 August 1999 Golcuk earthquake and big circles denote large earthquakes. Crosses show the distribution of seismicity in a 10-km-wide zone around the profile. The perturbation scale is shown to the right of each panel.

Fig. 14. The same as Fig. 13, but along line BB'.

cur close to zones characterized by average P wave velocity, low S wave velocity, and high Poisson's ratios (Figs. 11, and 12). In summary, a comprehensive analysis of tectonic landforms and associated structures, combining the results of seismic tomography and other geophysical observations, are valuable tools for defining the strain distribution pattern and its evolution in the near surface. These data are the basis for understanding how surface deformation builds up. Consequently, they provide a picture of the characteristics of the principal slip zone at depth,
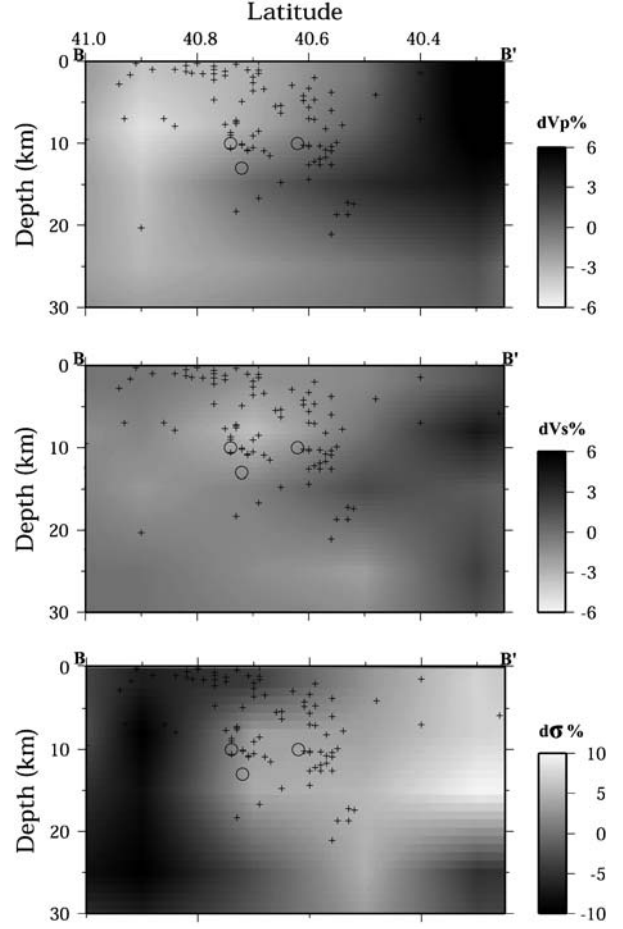
and are certainly of value for identifying and characterizing faults with potential for surface rupturing earthquakes.

5. 2 Previous geophysical observations and obtained velocity and Poisson's ratio models

The velocity models obtained in this study for western Anatolia are dominated by low velocities with the exception of a high-velocity anomaly at a depth of 8 km and by high Poisson's ratios (except at 25 km depth). The low Poisson's ratios at a depth of 25 km, which appear around the seismically active zone, have low or even no resolution, hence we consider them to be unreliable features. Akyol *et al.* (2006) obtained lower crustal velocities in western Anatolia and attributed them to high temperatures, fluids, and high pore pressure, or the presence of partial melt. Their results also reflect near-surface geological complexities and that crustal velocities are significantly slower in western Anatolia, increasing from 6.25 km/s at a depth of 21 km to only 6.43
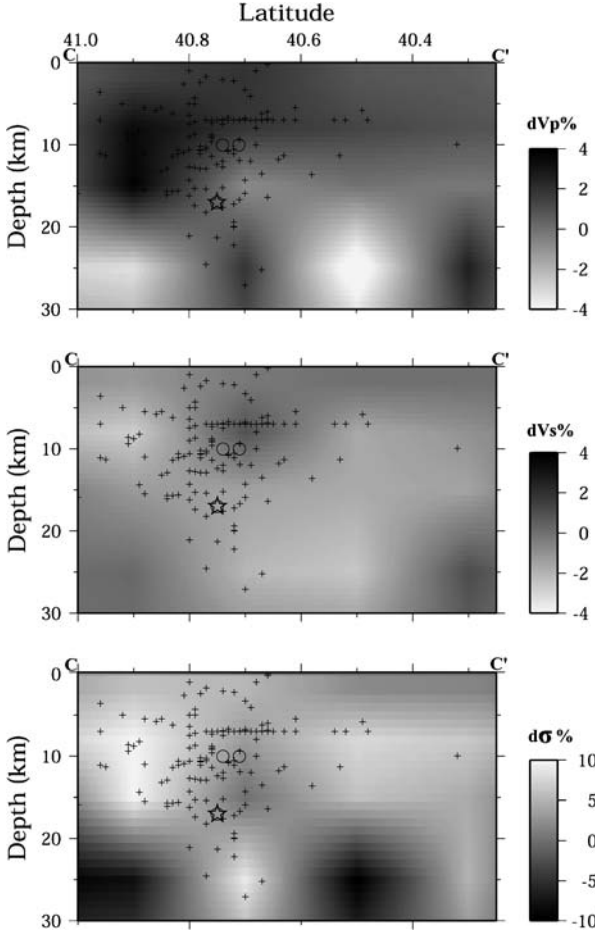
Fig. 15. The same as Fig. 13, but along line CC'.

Fig. 16. The same as Fig. 13, but along line DD'. The big cross denotes the hypocenter of the 12 November 1999 Düzce earthquake.

km/s at the Moho. The velocities obtained at the base of the crust are within the bounds of average crustal velocities at high temperatures (Christensen and Moony, 1995). These low velocities might indicate that fluid-filled faults and fractures in this seismically active region permeate the crust (*e.g.,* Al-Shukri and Mitchell, 1988; Mitchell *et al.,* 1997). It was also found that the average P_n velocity for the entire Aegean region is approximately 7.9 km/s (Panagiotopoulos and Papazachos, 1985), which is lower than the worldwide average continental upper mantle P_n velocity of 8.1 km/s (Moony and Braile, 1989).

Recently, Al-Lazki *et al.* (2004) detected broad-scale (∼500 km) zones of low (<8 km/s) P_n velocity anomalies underlying the Anatolian plate and the Anatolian plateau, and even smaller-scale ((∼200 km), very low (<7.8 km/s) P_n velocity zones beneath the Isparta Angle, central Turkey and the northern Aegean Sea region. The broad-scale low-velocity re-
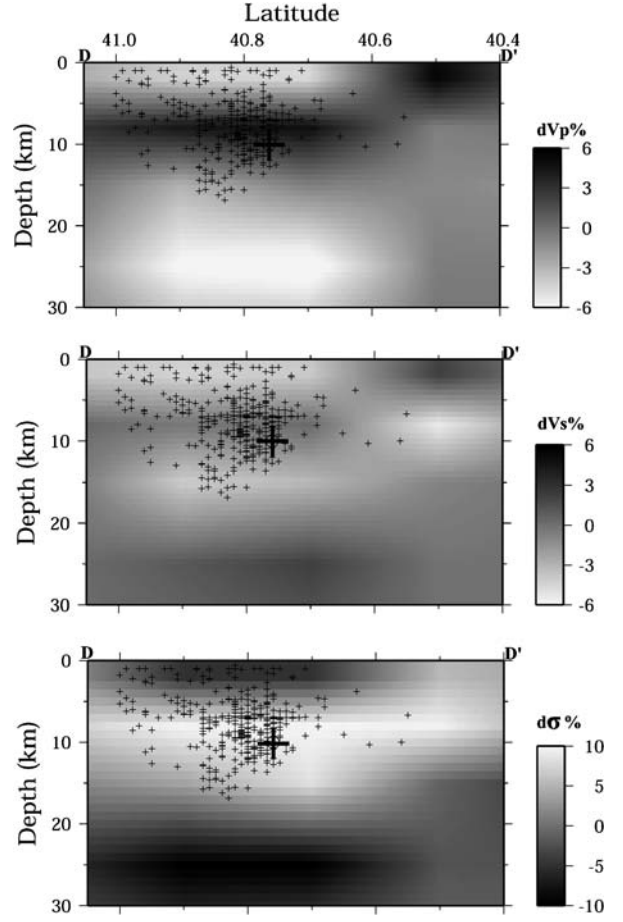
gions are interpreted to be hot and unstable mantle lid zones, whereas the very low P_n velocity zones are interpreted to be regions with no mantle lid. Although we have no resolution at depths greater than 25 km, these observations, however, support the existence of the low velocities and high Poisson's ratios anomalies we detected at depths greater than 15 km (Figs. 13–16). Seismic activity is concentrated mostly in the top 10 km depths, which might suggest the presence of seismically active low-angle breakaway faults within the upper crust of western Anatolia (Sengör, 1987).

Measurements of coda Q_c by Akinci *et al.* (1994) in western Anatolia for the frequency range 1.5–10 Hz show a strong frequency dependence, which agrees with the assumption that tectonically active areas show a high attenuation due to the complex structure of the region. Using a electrical resistivity sur-

vey in northwest Anatolia, Caglar (2001) detected a 5 km thick surface layer of low resistivity characterizing the sedimentary sequences of this depth range, and deduced that the tectonic structure is comparatively complex. Below a depth of about 5 km geoelectric models show a more resistive structure underlying these sediments. The resistive structure is correlated with Precambrian crystalline rocks and gneiss schist basement. This change from low to high resistivity at a depth of about 5 km is consistent with the change from low (at 2 km depth) to high (at 8 km depth) velocities we observed in our study. High average heat flow with geothermal activity (*e.g.,* Ilkisik, 1995; Pfister *et al.,* 1998; Gemici and Tarcan, 2002), high rate of seismicity (Bozkurt, 2001), intensive faulting and extension-related Neogene and Quaternary volcanism (*e.g.,* Paton, 1992; Innocenti *et al.,* 2005) are also among the main characteristics of the region.

Sari and Salk (2006) found that the most pronounced structural and morphological features in western Turkey are graben-like structures created by E-W normal faulting. The grabens are filled with recent sediments that give rise to relatively negative gravity anomalies. Caglar and Isseven (2004) detected three electrically conductive ($\sim$4–6 Ω m) zones at depths of 5–15 km. The origins of these zones are explained by the circulation of hydrothermal fluids with low resistivity values (0.28–0.52 Ω m) and by the effects of a strong hydrothermal alteration in the rocks. They also detected a low magnetic anomaly with a low intensity of about $<50\gamma$ in a central area in northwest Anatolia, and ascribed it to hydrothermal demagnetisation of the rocks due to geothermal activity.

6. Conclusions

In this study we collected a number of arrival times of P and S waves from the aftershocks of the two large 1999 earthquakes, as well as local earthquakes, and used them to map the 3-D crustal structure of P wave, S wave, and Poisson's ratio beneath northwest Anatolia. The velocity structure is very heterogeneous at shallow layers of the crust (2 and 8 km depths) with amplitudes of $\pm6\%$. It is dominated mainly by low velocities at a depth of 2 km and high velocities at a depth of 8 km. At the deepest layers of the crust (depths 15 and 25 km) most parts of the

study area are dominated by low velocity anomalies. Poisson's ratios are generally higher than average with minor patches of low Poisson's ratio anomalies. Seismic activity is concentrated near the zones characterized by low to average velocities and moderate to high Poisson's ratio. The results of a checkerboard resolution test show that most of the currently obtained structures are reliable features. They are also in general agreement with many other geophysical observations, although the scales of such studies should be considered. All these anomalies are associated with the complex and active tectonic setting of the region, the circulation of hot geothermal fluids, and the presence of sediment fillings at the surfacial layers.

The various pieces of evidence mentioned in the previous sections suggest that the generation of a large crustal earthquake is closely related to the surrounding tectonic environment such as rifting/spreading or the relative transform motion between adjacent plates and the physical/chemical properties of crustal materials such as magmas and fluids. Complex physical and chemical reactions may take place in the source zone of a future earthquake, causing heterogeneities in the material property and stress field, which may be detected by seismic tomography and other geophysical methods. These results indicate that large earthquakes do not occur anywhere, but only in anomalous areas that may be detected with geophysical methods. Higher resolution seismic imaging of this area combined with other geological, geochemical, and geophysical investigations would certainly deepen our understanding of the ongoing tectonic activity and the earthquake-generating processes, and would also contribute to the mitigation of seismic hazards.

References

Aki, K. and W. Lee, 1976, Determination of the three-dimensional velocity anomalies under a seismic array using first P arrival times from local earthquakes, 1.A homogeneous initial model, *J. Geophys. Res.,* **81**, 4381–4399.

Akinci, A., A.G. Taktak and S. Ergintav, 1994, Attenuation of coda waves in western Anatolia, *Phys. Earth Planet. Inter.,* **87**, 155–165.

Aktug, B. and A. Kiliçoglu, 2006, Recent crustal deformation of Izmir, western Anatolia and surrounding regions as deduced from repeated GPS measurements and strain field, *J. Geodyn.,* **41**, 471–484.

Akyol, N., L. Zhu, B.J. Mitchell, H. Sözbilir and K. Kekovalý, 2006, Crustal structure and local seismicity in western Anatolia, Geophys. J. Int., 10.1111/j.1365-246X.2006.03053.

Akyüz, H.S., A.A. Barka, E. Altunel, R.D. Hartleb and G. Sunal, 2000, Field observations and slip distribution of the November 12, 1999 Düzce earthquake (M＝7.1), Bolu-Turkey, in: the 1999 Izmit and Düzce earthquakes: Preliminary results, by A.A. Barka *et al.* (Ed.), pp. 63–70, Istanbul Tech. Univ., Istanbul.

Akyüz, H.S., R.D. Hartleb, A.A. Barka, E. Altunel, G. Sunal, B. Meyer and R. Armijo, 2002, Surface rupture and slip distribution of the 12 November 1999 Düzce earthquake (M 7.1), north Anatolian fault, Bolu, Turkey, *Bull. Seismol. Soc. Am.,* **92**, 61–66.

Al-Lazki, A.I., E. Sandvol, D. Seber, M. Barazangi, N. Turkelli and R. Mohamad, 2004, *Pn* tomographic imaging of mantle lid velocity and anisotropy at the junction of the Arabian, Eurasian and African plates, *Geophys. J. Int.,* **158**, 1024–1040.

Al-Shukri, H.J. and B.J. Mitchell, 1988, Reduced seismic velocities in the source zone of new Madrid earthquakes, *Bull. Seismol. Soc. Am.,* **78**, 1491–1509.

Ambraseys, N.N., 1970, Some characteristic features of the north Anatolian fault zone, *Tectonophysics,* **9**, 143–165.

Ambraseys, N.N., 2002, The seismic activity of the Marmara sea region over the last 2000 years, *Bull. Seismol. Soc. Am.,* **92**, 1–18.

Ambraseys, N.N. and C.F. Finkel, 1995, The seismicity of Turkey and adjacent areas: a historical review, 1500–1800. Muhittin Salih Eren, Istanbul, 240 pp.

Armijo, R., B. Meyer, A. Hubert and A.A. Barka, 1999, Westward propagation of the North Anatolian fault into the northern Aegean: Timing and kinematics, *Geology,* **27**, 267–270.

Ayhan, M.A., C. Demir, A. Kilicoglu, I. Sanli and S.M. Nakiboglu, 1999, Crustal motion around the western segment of the north Anatolian fault zone: Geodetic measurements and geophysical interpretation, paper presented at IUGG99, Int. Union of Geodesy and Geophys., Birmingham, U.K.

Barka, A.A., 1981, Seismo-tectonic aspects of the North Anatolian fault zone, Ph.D. thesis, 335 pp., Univ. of Bristol, Bristol, U.K.

Barka, A.A., 1992, The North Anatolian fault zone, Ann, *Tecton.,* **6**, 164–195.

Barka, A.A., 1999, The 17 August 1999 Izmit Earthquake, *Science,* **285**, 1858–1859.

Barka, A.A., H.S. Akyüz, E. Altunel, G. Sunal, Z. Çakir, A. Dikbas, B. Yerli, R. Armijo, B. Meyer, J.B. de Chabalier, T. Rockwell, J.R. Dolan, R. Hartleb, T. Dawson, S. Christofferson, A. Tucker, T. Furnal, R. Langridge, H. Stenner, W. Lettis, J. Bachhuber and W. Page, 2002, The surface rupture and slip distribution of the 17 August 1999 Izmit earthquake (M 7.4), north Anatolian fault, *Bull. Seismol. Soc. Am.,* **92**, 43–60.

Barka, A.A., H.S. Akyüz, H.A. Cohen and F. Watchorn, 2000, Tectonic evolution of the Niksar and Tasova-Erbaa pull-apart basins, north Anatolian fault zone: their significance for the motion of the Anatolian block, *Tectonophysics,* **322**, 243–264.

Barka, A.A. and L. Gülen, 1988, New constraints on age and total offset of the north Anatolian fault zone: Implications for tectonics of the eastern Mediterranean Region, In: Melih Tokay Symposium, Spec. Publ. Middle-east Techn. Univ., Ankara, pp. 39–65.

Barka, A.A. and P.L. Hancock, 1984, Neotectonic deformation patterns in the convex-northwards arc of the North Anatolian fault, in The Geological Evolution of the Eastern Mediterranean, edited by J.G. Dixon and A.H.F. Robertson, *Geol. Soc. Spec. Publ.,* **17**, 763–773.

Barka, A.A. and K. Kadinski-Cade, 1988, Strike-slip fault geometry in Turkey and its influence on earthquake activity, *Tectonophysics,* **7**, 663–684.

Bozkurt, E., 2001, Neotectonics of Turkey—a synthesis, *Geodyn. Acta,* **14**, 3–30.

Çaglar, I., 2001, Electrical resistivity structure of the northwestern Anatolia and its tectonic implications for the Sakarya and Bornova zones, *Phys. Earth Planet. Inter.,* **125**, 95–110.

Çaglar, I. and T. Isseven, 2004, Two-dimensional geoelectrical structure of the Göynük geothermal area, northwest Anatolia, Turkey, *J. Volcanol. Geother. Res.,* **134**, 183–197.

Canitez, N. and B. Üçer, 1967, Computer determinations for the fault plane solutions in and near Anatolia, *Tectonophysics,* **4**, 235–244.

Christensen, N., 1996, Poisson's ratio and crustal seismology, *J. Geophys. Res.,* **101**, 3139–3156.

Christensen, N. and W. Mooney, 1995, Seismic velocity structure and composition of the continental crust: a global view, *J. Geophys. Res.,* **100**, 9761–9788.

Gemici, Ü. and G. Tarcan, 2002, Hydrogeochemistry of the Simav geothermal field, western Anatolia, Turkey, *J. Volcanol. Geother. Res.,* **116**, 215–233.

Gürer, Ö.F., N. Kaymakçi, S. Çakir and M. Özburan, 2003, Neotectonics of the southeast Marmara region, NW Anatolia, Turkey, *J. Asian Earth Sci.,* **21**, 1041–1051.

Harvard, 1976–2002, CMT catalogue. http://www.seismology.harvard.edu/

Hirahara, K., 1977, A large-scale three-dimensional seismic structure under the Japan islands and the Sea of Japan, *J. Phys. Earth,* **25**, 393–417.

Hubert-Ferrari, A., R. Armijo, G. King, B. Meyer and A.A. Barka, 2002, Morphology, displacement, and slip rates along the northern Anatolian Fault, Turkey, *J. Geophys. Res.* **107** (B10), 2235, doi: 10.1029/2001JB000393.

Ilkisik, O.M., 1995, Regional heat flow in western Anatolia using silica temperature estimates from thermal springs, *Tectonophysics,* **244**, 175–184.

Innocenti, F., S. Agostini, G.D. Vincenzo, C. Doglioni, P. Manetti, M.Y. Savaşçin and S. Tonarini, 2005, Neogene and Quaternary volcanism in western Anatolia: Magma sources and geodynamic evolution, *Marine Geology,* **221**, 397–421.

Inoue, H., Y. Fukao, K. Tanabe and Y. Ogata, 1990, Whole mantle P wave travel time tomography, *Phys. Earth Planet. Inter.,* **59**, 294–328.

Kahle, H.G., M. Cocard, Y. Peter, A. Geiger, R. Reilinger, S.C. McClusky, R. King, A.A. Barka and G. Veis, 1999, The GPS strain rate field in the Aegean Sea and western Anatolia, *Geophys. Res. Lett.,* **26** (16), 2513–2516.

Kahle, H.G., M. Cocard, Y. Peter, A. Geiger, R. Reilinger, A.A. Barka and G. Veis, 2000, GPS-derived strain rate field within the boundary zones of the Eurasian, African, and Arabian plates, *J. Geophys. Res.,* **105** (B3), 23353–23370.

Kamiya, S. and Y. Kobayashi, 2000, Seismological evidence for the existence of serpentinized wedge mantle, *Geophys. Res. Lett.,* **27**, 819–822.

Kayal, J.R., D. Zhao, O.P. Mishra, R. De and O.P. Singh, 2002, The 2001 Bhuj earthquake: Tomographic evidence for fluids at the hypocenter and its implications for rupture nucleation, *Geophys. Res. Lett.,* **29**, 10.1029/ 2002GL015177.

McClusky, S.C., *et al.,* 2000, Global positioning system constraints on plate kinematics and dynamics in the eastern Mediterranean and Caucasus, *J. Geophys. Res.,* **105** (B3), 5695–5720.

Mckenzie, D.P., 1972, Active tectonics of the Mediterranean region, *Geophys. J. Roy Astron. Soc.,* **30**, 109–185.

Mishra, O.P., D. Zhao, N. Umino and A. Hasegawa, 2003, Tomography of northeast Japan forearc and its implications for interpolate seismic coupling, *Geophys. Res. Lett.,* **30** (16), 1850, doi: 10.1029/2003GL017736.

Mitchell, J.B., Y. Pan, J. Xie and L. Cong, 1997, *Lg* coda *Q* variation across Eurasia and its relation to crustal evolution, *J. Geophys. Res.,* **102**, 22767–22779.

Mooney, W.D. and L.W. Braile, 1989, The seismic structure of the continental crust and upper mantle of north America, In: The geology of north America: an overview, by A. Bally, P. Palmer (ed.), Geol. Soc. Am., Boulder, CO, pp. 39–52.

Muller, J.R, A. Aydin and F. Maerten, 2003, Investigating the transition between the 1967 Mudurnu Valley and 1999 Izmit earthquakes along the north Anatolian fault with static stress changes, *Geophys. J. Int.,* **154**, 471–482.

Nakajima, J., T. Matsuzawa, A. Hasegawa and D. Zhao, 2001, Three-dimensional structure of Vp, Vs, and Vp/Vs beneath northeastern Japan: implications for arc magmatism and fluids, *J. Geophys. Res.,* **106**, 21843–21857.

Nakajima, J., Y. Takei and A. Hasegawa, 2005, Quantitative analysis of the inclined low-velocity zone in the mantle wedge of northeastern Japan: a systematic change of melt-filled pore shapes with depth and its implications for melt migration, *Earth Planet. Sci. Lett.,* **234**, 59–70.

National Earthquake Information Center (NEIC), 2006, http://neic.usgs.gov/neis/epic/epic_rect.html.

Panagiotopulos, D.G. and B.C. Papazachos, 1985, Travel times of Pn waves in the Aegean and surrounding area, *Geophys. J. R. Astron. Soc.,* **80**, 165–176.

Papazachos, B.C., A.S. Savvaidis, G.F. Karakaisis and C.B. Papazachos, 2002, Precursory accelerating seismic crustal deformation in the northwestern Anatolia fault zone, *Tectonophysics,* **347**, 217–230.

Paton, S., 1992, Active normal faulting, drainage patterns and sedimentation in southwestern Turkey, *J. Geol. Soc. Lond.,* **149**, 1031–1044.

Pfister, M., L. Rybach and S. Simsek, 1998, Geothermal reconnaissance of the Marmara Sea region (NW Turkey): surface heat flow density in an area of active continental extension, *Tectonophysics,* **291**, 77–89.

Provost, A.-S., J. Chéry and R. Hassani, 2003, 3-D mechanical modeling of the GPS velocity field along the North Anatolian Fault, *Earth Planet. Sci. Lett.,* **209**, 361–377.

Pucci, S., N. Palyvos, C. Zabci, D. Pantosti and M. Barchi, 2006, Coseismic ruptures and tectonic landforms along the Duzce segment of the north Anatolian fault zone (Ms 7.1, November 1999), *J. Geophys. Res.,* **111**, doi: 10. 1029/2004JB003578.

Reilinger, R.E., S.C. McClusky, M.B. Oral, W. King and M.N. Toksöz, 1997, Global positioning system measurements of present-day crustal movements in the Arabian-Africa-Eurasia plate collision zone, *J. Geophys. Res.,* **102** (B5), 9983–9999.

Reilinger, R.E., M.N. Toksöz, S.C. McClusky and A.A. Barka, 2000, 1999 Izmit, Turkey Earthquake was no surprise, *GSA Today,* **10**, 1–6.

Rockwell, T., A.A. Barka, T. Dawson, S. Akyüz and K. Thorup, 2001, Paleoseismology of the Gazikoy-Saros segment of the north Anatolian fault, northwestern Turkey: Comparison of the historical and paleoseismic records, implications of regional seismic hazard, and models of earthquake recurrence, *J. Seismol.,* **5**, 433–448.

Salah, M.K. and D. Zhao, 2003, 3-D seismic structure of Kii Peninsula in southwest Japan: evidence for slab dehydration in the forearc, *Tectonophysics,* **364**, 191–213.

Sari, C. and M. Salk, 2006, Sediment thicknesses of the western Anatolia graben structures determined by 2D and 3D analysis using gravity data, *J. Asian Earth Sci.,* **26**, 39–48.

Saroglu, F., Ö. Emre and I. Kusçu, 1992, Active fault map of Turkey, map, Gen. Dir. of Miner. Res. and Explor., Ankara.

Sengör, A.M.C., 1979, The north Anatolian transform fault: its age, offset and tectonic significance, *J. Geol. Soc. London,* **136**, 269–282.

Sengör, A.M.C. 1987, Cross-faults and differential stretching of hanging walls in regions of low-angle normal faulting: examples from western Turkey, *Spec. Publ. Geol. Soc. London,* **28**, 575–589.

Serrano, I., F. Bohoyo, J. Galindo-Zaldivar, J. Morales and D. Zhao, 2002a, Geophysical signatures of a basic-body rock placed in the upper crust of the external zones of the Betic Cordillera (Southern Spain), *Geophys. Res. Lett.,* **29** (11), doi: 10.1029/2001GL013487.

Serrano, I., J. Morales, D. Zhao, F. Torcal and F. Vidal, 1998, P-wave tomographic images of the central Betics Alboran sea (South Spain) using local earthquakes: contribution for a continental collision, *Geophys. Res. Lett.,* **25** (21), 4031-4034, 10.1029/1998GL900021.

Serrano, I., D. Zhao and J. Morale, 2002b, 3-D crustal structure of the extensional Granada basin in the conver-

gent boundary between the Eurasia and African plates, *Tectonophysics,* **344**, 61–79.

Seymen, I., 1975, Tectonic characteristics of the North Anatolian Fault Zone in the Kelkit valley, Ph.D. thesis, 192 pp., Istanbul Tech. Univ., Istanbul.

Spakman, W. and G. Nolet, 1988, Imaging algorithms, accuracy and resolution in delay time tomography, In: Vlaar, N. J., *et al.* (Eds.), Mathematical Geophysics, D. Reidel, Norwell, MA, pp. 155–187.

Straub, C., H.G. Kahle and C. Schindler, 1997, GPS and geologic estimates of the tectonic activity in the Marmara Sea region, NW Anatolia, *J. Geophys. Res.,* **102** (B12), 27587–27601.

Takei, Y., 2002, Effect or pore geometry on Vp/Vs: from equilibrium geometry to crack, *J. Geophys. Res.,* **107**, 10. 1029/2001JB000522

Thurber, C.H., 1983, Earthquakes locations and three-dimensional crustal structure in the Coyote Lake area, Central California, *J. Geophys. Res.,* **88**, 8226–8236.

Tibi, R., G. Bock, Y. Xia, M. Baumbach, H. Grosser, C. Milkereit, S. Karakisa, S. Zünbül, R. Kind and J. Zschau, 2001, Rupture process of the 1999 August 17 Izmit and November 12, 1999 Düzce (Turkey) earthquakes, *Geophys. J. Int.,* **144**, F1–F7.

Tokay, M., 1973, Geological observation on the north Anatolian fault zone between Gerede and Ilgaz, paper presented at Symposium on the North Anatolian Fault Zone and Earthquake Belt, Miner. Res. and Explor. Inst. of Turkey, Ankara.

USGS- United States Geological Survey, Implication for earthquake risk reduction in the United States from the Kocaeli. Turkey earthquake of August 17.1999, US Geological Survey Circular 1193: 1999.

Utkucu, M., S.S. Nalbant, J. McCloskey, S. Steacy and O. Alptekin, 2003, Slip distribution and stress changes associated with the 1999 November 12, Duzce (Turkey) earthquake (Mw＝7.1), *Geophys. J. Int.,* **153**, 229–241.

Wessel, P. and W.H.F. Smith, 1998, New improved version of Generic Mapping Tools released, *EOS Trans. Am. Geophys. Union,* **79**, 579.

Westaway, R., 1994, Present-day kinematics of the middle east and eastern Mediterranean, *J. Geophys. Res.,* **99** (B6), 12071–12090.

Zanchi, A. and J. Angelier, 1993, Seismotectonics of western Anatolia: regional stress orientation from geophysical and geological data, *Tectonophysics,* **222**, 259–274.

Zhao, D., A. Hasegawa and S. Horiuchi, 1992, Tomographic imaging of P and S wave velocity structure beneath northeastern Japan, *J. Geophys. Res.,* **97**, 19909–19928.

Zhao, D., A. Hasegawa and H. Kanamori, 1994, Deep structure of Japan subduction zone as derived from local, regional and teleseismic events, *J. Geophys. Res.,* **99**, 22313–22329.

Zhao, D. and H. Kanamori, 1995, The 1994 Northridge earthquake: 3-D crustal structure in the rupture zone and its relation to the aftershock locations and mechanisms, *Geophys. Res. Lett.,* **22**, 763–766.

Zhao, D., H. Kanamori and H. Negishi, 1996, Tomography of source area of the 1995 Kobe earthquake: evidence for fluids at the hypocenter?, *Science,* **274**, 1891–1894.

Zhao, D. and H. Negishi, 1998, The 1995 Kobe earthquake: seismic image of the source zone and its implications for the rupture nucleation, *J. Geophys. Res.,* **103**, 9967–9986.

Zhao, D., K. Wang, G.C. Rogers and S.M. Peacock, 2001, Tomographic image of low P velocity anomalies above slab in northern Cascadia subduction zone, *Earth Planets Space,* **53**, 285–293.

Zhao D., Y. Xu, D.A. Wiens, L.M. Dormon, J. Hildebrend and J. Webb, 1997, Depth extent of the Lau backarc spreading center and its relationship to subduction processes, *Science,* **278**, 254–257.

Zhou, H. and R.W. Clayton, 1990, P and S wave travel time inversions for subducting slab under the island arcs of northwest Pacific, *J. Geophys. Res.,* **95**, 6829–6851.